Progress In Electromagnetics Research, PIER 80, 123–160, 2008

HANDSET ANTENNA DESIGN: PRACTICE AND THEORY

W. Geyi, Q. Rao, S. Ali, and D. Wang

Research In Motion
185 Columbia St. W., Waterloo, Ontario, Canada, N2L 5Z5

Abstract—In this paper, an attempt is made to present a theory for the design of handset antennas, which results from the long experience that the authors have in the field of handset antenna design. The proposed theory is based on the well-known skin effect and constructs the antenna using a thin wire model that represent the backbone of the final antenna. The analytical solution for the thin wire model is first obtained, and the main properties (such as the return loss and the radiation properties) of the antenna can then be studied using this analytical solution. Once the antenna backbone is constructed, other elements, such as stubs, patches, etc., can be added to optimize the match at the desired frequency bands. A number of numerical and analytical examples are provided throughout the paper to validate the theory. Different antenna types, such as wire antennas and planar antennas, are tested and designed using the thin wire model. The correspondence between the analytical results and those from the numerical simulations using full-wave solvers agree very well in all examples. The authors also present in this paper a novel design of three small antennas for handset applications, which are based on the simple wire monopole, but in a three-dimensional form. The proposed three-dimensional monopole antennas have multi-band and broadband properties that cover most frequency bands being used for the handset device. The antennas feature remarkable properties while occupying a significantly small space, which makes them strong candidates for handset applications and for the future multi-antenna applications too.

1. INTRODUCTION

In the early 20th century, mobile technology had been predominated by military users. Before World War II, most developed mobile communications were dedicated to military requirements and

standards. In fact, the first wireless telecommunication systems were heavy and large that their equipment would occupy the trunk of the car carrying the device. Additionally, the required power to operate these systems was high leading to a very poor battery life [1]. A revolution in the telecommunications and in the information technologies, and hence the mobile communications technology, was witnessed in the early nineteen nineties after the advent of microelectronics [1, 2]. The breathtaking growth of the wireless internet, with traffic continuing to double annually as witnessed in the last decade of the last century, makes an epitome of this revolutionary trend [2]. With this revolution, mobile communication devices became lighter, smaller, and consumed less power to operate [3]. In all this, industry and researches came to understand the role of electromagnetic field theory, or specifically the role of the antenna element, as a key role in this growing trend. The antenna is the electromagnetic transducer which is used to convert, in the transmitting mode, a guided wave within a transmission line to radiated wave in the free-space. In the receiving mode, the antenna converts the free-space wave into guided wave [4]. A good antenna design can relax the system requirements and improve the overall system performance.

Wire antennas, such as the monopole and the modified monopole antennas (see Figure 1), were the first type of antennas recognized for mobile communication devices. They are easy to design, light weight, and have omni-directional radiation pattern in the horizontal plane [5]. However, since the physical length of a monopole antenna is quarter of its wavelength at the operating frequency, this antenna is relatively very long. Therefore, monopole antennas are usually external antennas. As the size of handheld devices was decreasing, the inverted-L antenna (ILA) was found to be a promising alternative to replace the external monopole antenna. The ILA is an end-fed short monopole

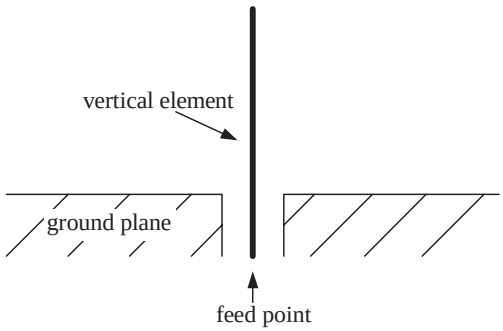

Figure 1. Fundamental structure of the monopole antenna.

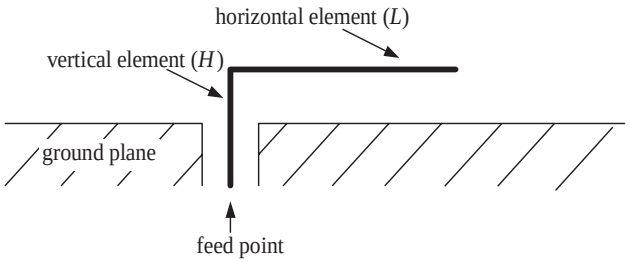

Figure 2. Inverted-L antenna (ILA) modified from the monopole antenna.

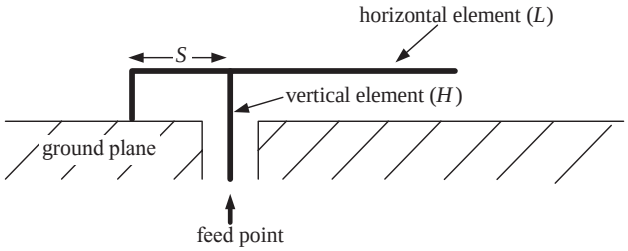

Figure 3. Inverted-F antenna (IFA) modified from the ILA.

with a horizontal wire element placed on top that acts as a capacitive load (see Figure 2). The design of the ILA has a simple layout making it cost efficient to manufacture [3]. Although the radiation properties of the ILA have advantages over those of the monopole antenna by radiating in both polarizations due to the horizontal arm, however, its input impedance is similar to that of the short monopole: low resistance and high reactance. This prompted antenna designers to search for an antenna with nearly resistive load thus provides reduced mismatch loss. For this purpose, the inverted-F antenna (IFA) was introduced (see Figure 3) [6, 7], which adds a second inverted-L section to the end of an ILA. The additional inverted-L segment introduces a convenient tuning option to the original ILA and greatly improves the antenna usability. Even with the improvement in the match of the IFA over the ILA, both these antennas have inherently narrow bandwidths. To obtain broad bandwidth characteristics, antenna designers transformed the horizontal element from a wire to a plate (see Figure 4), and the planar inverted-F antenna (PIFA) was introduced [8]. The PIFA is widely used in nowadays mobile handheld devices. It is a self-resonating antenna with purely resistive impedance at the frequency of operation. This makes it a practical candidate for mobile handheld design since it does not require a conjugate circuit between

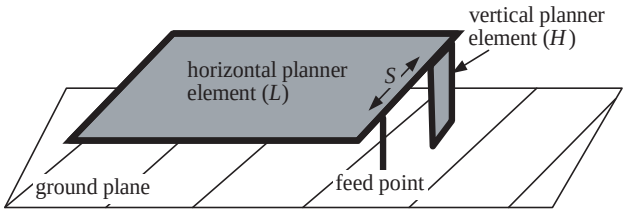

Figure 4. Basic layout of the planar inverted-F antenna (PIFA) modified from the IFA.

the antenna and the load reducing both cost and losses. Despite the relative simple design of the ILA, IFA, and the PIFA, the optimal design of any of these antennas is not unique (see Figures 2–4). Variations in the height of the radiator (H), the length of the horizontal element (L), the distances and the location of the feed and the shorting point (S), etc. all affect the electrical performance of these antennas. Numerous designs have been reported in the literature, e.g., [5–18]. Many of them suggest approaches to further improve the bandwidth and the performance of these antennas, e.g., [9, 18]. To the best of our knowledge, there has been no theory that can describe the behavior or the design procedure of these antennas. The best that can be found in the literature is some design recommendations based on the trial and error procedures that take place in the antenna laboratories while building the antenna prototypes or from the numerical simulations.

The evolution of the handset antenna designs from a monopole to the PIFA indicates that that the essential component of a handset antenna is the "wire". The patch(s) slot(s), and stub(s) are only used to compensate for the mismatch and improve the radiation characteristics. Notice that at the megahertz frequency range, the current flowing on the surface of a conductor no longer has a uniform distribution due to the skin effect, but it is confined to a relatively small area. Therefore, the effective cross-sectional area of the conductor is smaller than the actual dimension [19]. For example, by simulating a basic PIFA and examining the current distribution on its surface at the frequency of operation, one can see that the current distribution is concentrated at the edge(s) of some of the antenna parts. Therefore, the length of these edge(s) where the current is concentrated is the major parameter that tunes the antenna to that desired frequency [3, 10]. The remainder of the conductor plate(s) forming the patch(s) of that antenna part is, therefore, not an essential part in tuning the antenna but are rather to improve the antenna characteristics. In fact, removing these parts would affect the matching of the antenna

and would not detune it much. From this intuition, we propose a new procedure in handset antenna design. As a first step in the design, we represent the antenna by the fundamental wires responsible for its tuning at the frequencies of operation, and these become the backbone of the final design. We then derive an analytical solution for this wire model representation. Using this analytical solution, the antenna designer can easily and efficiently design the antenna that is tuned to the desired frequency by only solving a few analytical equations, no simulations or prototypes are required. The designer can further improve the basic design by adding patch(s), stub(s), slot(s) or a combination of these to reduce the mismatch and to improve the radiation characteristics.

Using the wire model to represent the antenna raises a question — would it be possible to achieve multi-band operation with broadband performance using the "wire" only? We have come to find the answer to this question by introducing a three-dimensional (3D) monopole antenna. This novel design has the virtues of simplicity and smaller maximum size than any known handset antenna design to date. The PIFA has been considered to be the most favorable antenna for handheld devices. However, our novel design outperforms the PIFA for a given maximum antenna size. It has a remarkably wider bandwidth, an impressively simpler structure, and its performance is less affected by the environment compared to the PIFA.

The paper is organized as follows: The validity of the thin wire model for the handset antenna is demonstrated in Section 2, where a PIFA antenna is examined and its equivalent wire model is presented. This example shows the equivalence between the original PIFA and the thin wire model. Section 3 gives a detailed derivation of the analytical solutions for some typical thin wire models, which are validated by comparisons with simulation results using full-wave MoM-based simulations [20, 21]. Discussions on the antenna bandwidth improvements by bending or wrapping the antenna in a 3D manner are introduced in Section 4. In Section 5, the novel 3D monopole antenna designs are discussed through three examples, which cover at least GSM, UMTS, and the higher WiMAX bands while the maximum dimension is kept very small [22–24].

2. WIRE MODELS FOR HANDSET ANTENNAS: AN EXAMPLE

To illustrate the idea of the thin wire model, we introduce a numerical example of a PIFA and represent it with its equivalent thin wire model. Consider the antenna shown in Figure 5(a) [25–29]. The equivalent

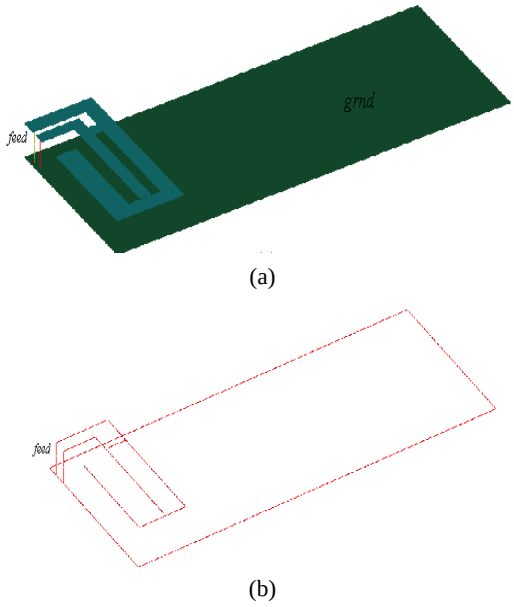

Figure 5. A typical PIFA: (a) planar model, and (b) equivalent thin wire model.

wire model for this antenna is shown in Figure 5(b) where the planar surface of the antenna is replaced by a wire along its outer edges. The radius of the wire can be very small, here we choose $a/\lambda = 10^{-4}$. The ground plane is replaced by an equivalent wire loop that is connected to the wire antenna model at the feed and at the shorting points, respectively. A key factor in the design of an antenna is the current distribution on its surface. This distribution can provide information on the resonating element(s), and hence, the controlling element(s), at each frequency of interest. These elements become design parameters in tuning the antenna. Both the planar structure and the wire models of the antenna shown in Figure 5 are simulated using the commercial full-wave electromagnetic solver FEKO [20]. The results showing the current distributions in both models at two different frequencies are given in Figures 6 and 7, respectively.

Notice that the intensity of the current distribution on the ground plane is stronger at the lower frequency than that at the higher frequency, see Figures 6(a) and 7(a), respectively. This states that the ground plane is actually part of the antenna at this frequency. The same can be concluded from the corresponding wire model, see Figures 6(b) and 7(b), respectively.

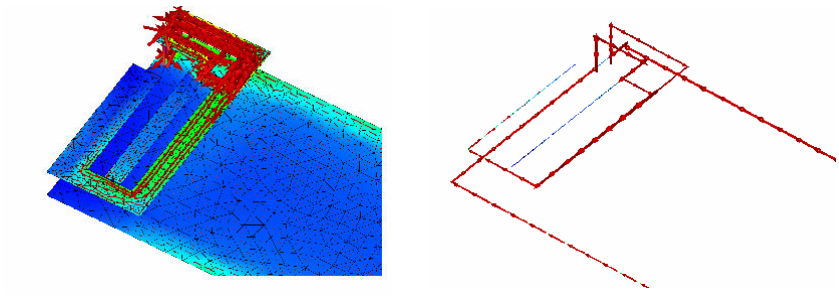

(a) (b)

Figure 6. Current distribution at the low frequency band: (a) the actual planar structure (b) the equivalent thin wire model.

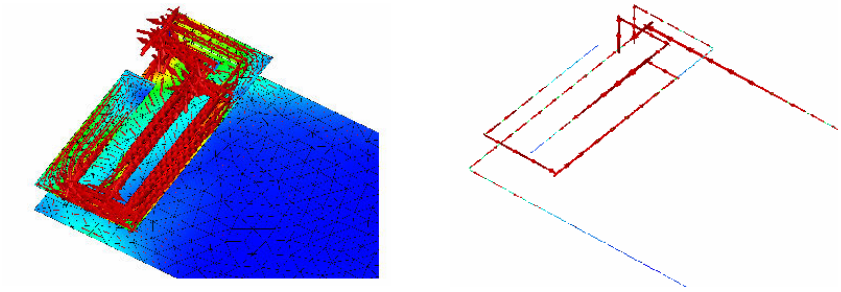

(a) (b)

Figure 7. Current distribution at the high frequency band: (a) the actual planar structure (b) the equivalent thin wire model.

The correspondence between the current distribution in the planar model and in the wire model is analogous in terms of direction and intensity at both the low and the high frequencies. Hence, one can expect that the radiation properties of both models are similar. Figures 8 and 9 show the radiation properties for both models at the two different frequencies of interest. Again, the correspondence between the results in the two models is analogous, which verifies the equivalence of thin wire model to the original planar antenna structure.

The thin wire model can give accurate information on the radiation properties of the original planar antenna. However, this model does not provide information on the matching of the antenna, hence, the impedance values may vary between the two models. Figure 10 shows the simulated return loss of the planar antenna and its equivalent wire model. The results show that the wire model can

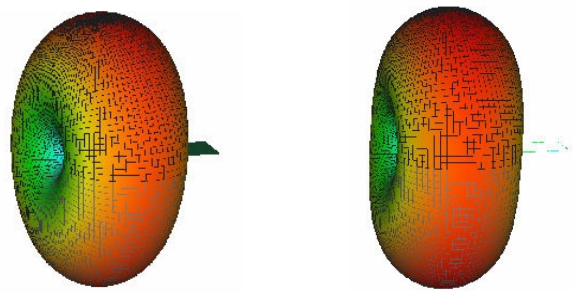

(a) (b)

Figure 8. Simulated radiation pattern at 900 MHz for: (a) the planar antenna model (b) the thin wire antenna model.

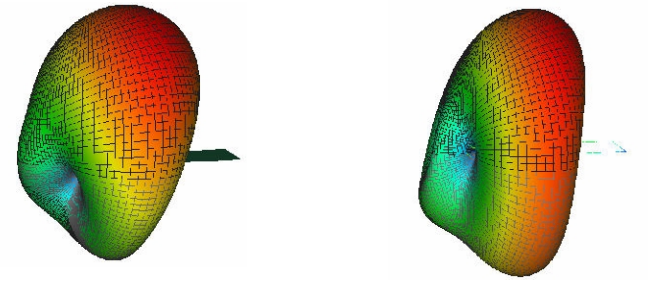

(a) (b)

Figure 9. Simulated radiation pattern at 1800 MHz for: (a) the planar antenna model, and (b) the thin wire antenna model.

provide a good, fast, and a simple starting point for the design of this antenna.

3. ANALYTICAL SOLUTIONS FOR THIN WIRE MODELS

Now it is clear that the main features of a metal handset antenna can be characterized by a very thin wire model, which is based on the well-known skin effect. The wire structures have been extensively investigated by a number of authors [e.g., 30, 31]. When the radius of the wire model for a handset antenna is very thin, it is possible to find an analytical solution for the current distribution on the wire, which includes useful information on the radiation properties of the original metal handset antenna. Thus, it provides guidelines for practical

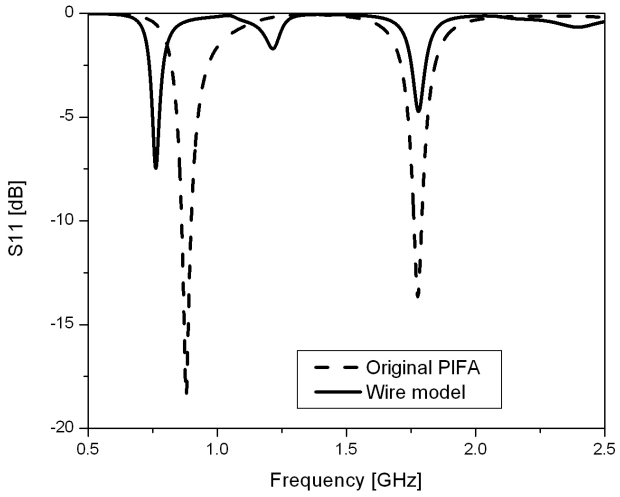

Figure 10. Simulated return loss for the PIFA and its equivalent thin wire model.

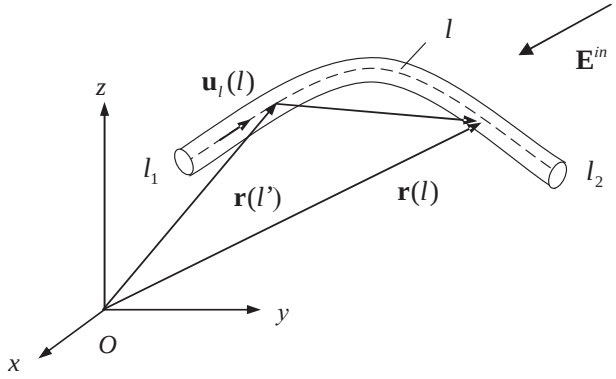

Figure 11. An arbitrary wire illuminated by an incident field.

handset antenna design. Let us consider a thin wire illuminated by an incident field $\boldsymbol{E}^{in}$. We assume that the wire is a curved circular cylinder of radius a and a curvilinear l-axis (l stands for arc length) runs along the axis of the circular cylinder as shown in Figure 11. The scattered field due to the current in the wire is $\boldsymbol{E}^{sc}(\boldsymbol{r}) = -j\omega\boldsymbol{A} - \nabla\phi$, where $\boldsymbol{A}$ is the vector potential and ϕ is the scalar potential. On the surface of the wire we have $\boldsymbol{E}^{in} + \boldsymbol{E}^{sc} = 0$. Thus

$$\boldsymbol{E}^{in} = -\boldsymbol{E}^{sc} = j\omega\boldsymbol{A} + \nabla\phi \tag{1}$$

Let $\boldsymbol{u}_l(l)$ be the unit tangent vector along l-axis. Multiplying both sides of (1) by $\boldsymbol{u}_l(l)$ leads to

$$\boldsymbol{E}^{in} \cdot \boldsymbol{u}_l(l) = j\omega \boldsymbol{A} \cdot \boldsymbol{u}_l(l) + \frac{d\phi}{dl} \tag{2}$$

The vector potential $\boldsymbol{A}$ on the surface of the wire due to a current distribution $I(l)$ is given by

$$\boldsymbol{A}(\boldsymbol{r}) = \frac{\mu}{2\pi} \int_0^{2\pi} d\varphi \int_{l_1}^{l_2} I(l')\boldsymbol{u}_l(l') \frac{e^{-jkR}}{4\pi R} dl'$$

where φ is the polar angle of a polar coordinate system whose origin is at the center of the cross section of the circular wire, and $R = |\boldsymbol{r}(l) - \boldsymbol{r}(l')|$. Since the integrand is singular at $l' = l$, we rewrite the above as

$$\begin{aligned}\boldsymbol{A}(\boldsymbol{r}) = {} & \frac{\mu}{2\pi}\int_0^{2\pi} d\varphi \int_{l_1}^{l-\tau} I(l')\boldsymbol{u}_l(l') \frac{e^{-jkR}}{4\pi R} dl' \\ & + \frac{\mu}{2\pi} \int_0^{2\pi} d\varphi \int_{l-\tau}^{l+\tau} I(l')\boldsymbol{u}_l(l') \frac{e^{-jkR}}{4\pi R} dl' + \frac{\mu}{2\pi}\int_0^{2\pi} d\varphi \int_{l+\tau}^{l_2} I(l')\boldsymbol{u}_l(l') \frac{e^{-jkR}}{4\pi R} dl'\end{aligned} \tag{3}$$

where τ is positive number. The second term on the right-hand side can be written as

$$\begin{aligned}\frac{\mu}{2\pi}\int_0^{2\pi} d\varphi \int_{l-\tau}^{l+\tau} I(l')\boldsymbol{u}_l(l') \frac{e^{-jkR}}{4\pi R} dl' &= \frac{\mu}{2\pi}\boldsymbol{u}_l(l)I(l) \int_0^{2\pi} d\varphi \int_{l-\tau}^{l+\tau} \left(\frac{1}{4\pi R} + \frac{e^{-jkR}-1}{4\pi R}\right) dl' \\ = \frac{\mu}{2\pi}\boldsymbol{u}_l(l)I(l) \int_0^{2\pi} d\varphi \int_{l-\tau}^{l+\tau} \frac{1}{4\pi R} dl' &+ \frac{\mu}{2\pi}\boldsymbol{u}_l(l)I(l) \int_0^{2\pi} d\varphi \int_{l-\tau}^{l+\tau} \frac{\cos kR - 1}{4\pi R} dl' \\ & - j\frac{\mu}{2\pi}\boldsymbol{u}_l(l)I(l) \int_0^{2\pi} d\varphi \int_{l-\tau}^{l+\tau} \frac{\sin kR}{4\pi R} dl'\end{aligned} \tag{4}$$

where $R = |\boldsymbol{r} - \boldsymbol{r}'| = [(l-l')^2 + \alpha^2]^{1/2}$, $\alpha^2 = 4a^2 \sin^2(\varphi - \varphi')/2$ if τ is not very big. Making use of the following asymptotic calculations for

small τ [30]

$$\int_0^{2\pi} d\varphi \int_{l-\tau}^{l+\tau} \frac{1}{4\pi R} dl' = \ln 2\tau - \ln a \tag{5}$$

$$\int_0^{2\pi} d\varphi \int_{l-\tau}^{l+\tau} \frac{\cos kR - 1}{4\pi R} dl' = Ci(k\tau) - \ln k\tau - \gamma \tag{6}$$

$$\int_0^{2\pi} d\varphi \int_{l-\tau}^{l+\tau} \frac{\sin kR}{4\pi R} dl' = \int_0^{\tau} \frac{\sin ku}{u} du \tag{7}$$

(4) can be written as

$$\begin{aligned} &\frac{\mu}{2\pi} \int_0^{2\pi} d\varphi \int_{l-\tau}^{l+\tau} I(l') \boldsymbol{u}_l(l') \frac{e^{-jkR}}{4\pi R} dl' \\ &= \frac{\mu}{2\pi} \boldsymbol{u}_l(l) I(l) (\ln 2\tau - \ln a) + \frac{\mu}{2\pi} \boldsymbol{u}_l(l) I(l) [Ci(k\tau) - \ln k\tau - \gamma] \\ &\quad -j \frac{\mu}{2\pi} \boldsymbol{u}_l(l) I(l) \int_0^{\tau} \frac{\sin ku}{u} du = -\frac{\mu}{2\pi} \boldsymbol{u}_l(l) I(l) \ln ka + \text{finite numbers} \end{aligned} \tag{8}$$

As $a \to 0$, the first and third term on the right-hand side of (3) are finite numbers. Thus

$$\boldsymbol{A}(\boldsymbol{r}) = -\frac{\mu}{2\pi} \boldsymbol{u}_l(l) I(l) \ln ka \tag{9}$$

From Lorentz gauge condition $\nabla \cdot \boldsymbol{A} + j\omega\mu\varepsilon\phi = 0$, we may find that

$$\frac{d\boldsymbol{A} \cdot \boldsymbol{u}_l(l)}{dl} + j\omega\mu\varepsilon\phi = 0 \tag{10}$$

It follows from (2), (9) and (10) that

$$\begin{aligned} \frac{d\phi}{dl} + j\omega L_0 I(l) &= \boldsymbol{E}^{in} \cdot \boldsymbol{u}_l(l) \\ \frac{dI(l)}{dl} + j\omega C_0 \phi &= 0 \end{aligned} \tag{11}$$

where $L_0 = -\frac{\mu}{2\pi} \ln ka,\ C_0 = \frac{\mu\varepsilon}{L_0}$. From (11) we obtain

$$\frac{d^2 I(l)}{dl^2} + k^2 I(l) = -j\omega C_0 \boldsymbol{E}^{in} \cdot \boldsymbol{u}_l(l) \tag{12}$$

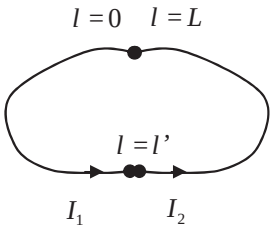

Figure 12. An arbitrary loop antenna excited by a delta gap.

where $k = \omega\sqrt{\mu\varepsilon}$. Since we have assumed that the wire is very thin, the source term $\boldsymbol{E}^{in} \cdot \boldsymbol{u}_l(l)$ in (12) can be replaced by a delta function

$$\frac{d^2 I(l)}{dl^2} + k^2 I(l) = -j\omega C_0 \delta(l - l') \tag{13}$$

We now give the analytical solutions for some typical wire structures.

3.1. Loop Antenna

Let us consider a loop antenna excited by a delta gap at $l = l'$ as shown in Figure 12. In this case, the boundary condition $I(0) = I(L)$ must be applied. The general solution of (13) can be written as

$$I(l) = \begin{cases} I_1 = C_1 \cos kl + C_2 \sin kl, & 0 < l < l' \\ I_2 = C_3 \cos kl + C_4 \sin kl, & l' < l < L \end{cases}$$

Making use of the facts that the current and its derivative must be continuous at $l = 0$, and

$$\left.\frac{dI_2}{dl}\right|_{l=l'+} - \left.\frac{dI_1}{dl}\right|_{l=l'-} = -j\omega C_0$$

We may find that the current distribution of a thin loop is given by

$$I(l) = \frac{j\pi}{\eta \ln ka} \frac{\cos\dfrac{k}{2}(L - 2|l - l'|)}{\sin\left(k\dfrac{L}{2}\right)} \tag{14}$$

where we have used $\frac{\omega C_0}{k} = -\frac{2\pi}{\eta \ln ka}$.

In order to verify the analytic solution for the loop antenna, equation (14) is applied to calculate the current distribution of a

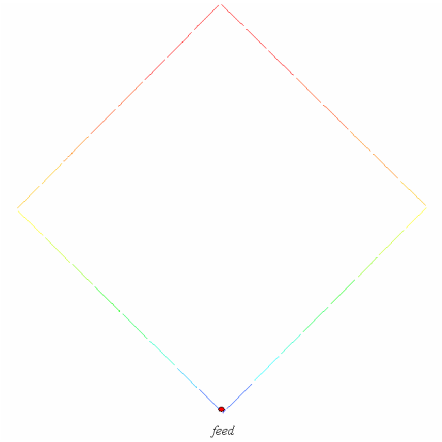

Figure 13. A half-wavelength rhombic loop antenna and the simulated current amplitude distribution by FEKO.

half-wavelength rhombic loop antenna, whose structure is shown in Figure 13. The calculated values are compared with the simulated ones using FEKO. The results show a very good agreement and are plotted in Figure 14. It should be noted that Figure 14 only shows the current distribution on a half of the rhombic loop antenna due to symmetrical nature of the structure. The maximum value of the current amplitude is at the center of the loop, i.e., 0.25 wavelength away from the feed at the corner. The minimum current can be found at the feed (see the current intensity shown in Figure 13). Since the current phase distribution along the loop is only related to its electrical length, the same phase distribution is obtained in the two models.

3.2. Dipole Antenna

Our second example is an arbitrary dipole excited by a delta gap at $l = l'$ as shown in Figure 15.

The current distributions along the two arms can be written as

$$I(l) = \begin{cases} I_1 = C_1 \cos kl + C_2 \sin kl, & 0 < l < l' \\ I_2 = C_3 \cos kl + C_4 \sin kl, & l' < l < L \end{cases}$$

From $I(0) = I(L) = 0$ and the source condition, we may find that the current distribution for the dipole is given by

$$I(l) = -\frac{j\pi}{\eta \sin kL \ln ka}[-\cos k(L - |l - l'|) + \cos k(L - l - l')] \quad (15)$$

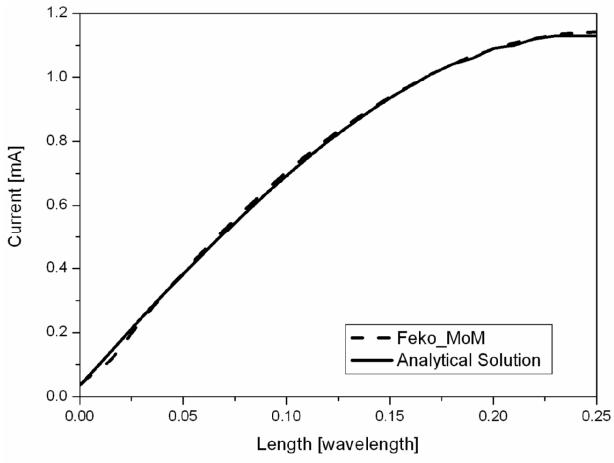

Figure 14. Current distributions for the rhombic loop antenna.

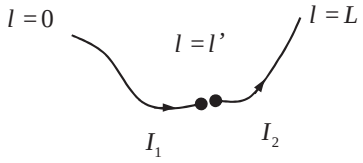

Figure 15. An arbitrary dipole antenna excited by a delta gap.

Equation (15) has been applied to calculate the current distribution of the quarter-wavelength dipole antenna shown in Figure 16. The obtained results from (15) are compared with the simulated ones using FEKO. A good agreement is obtained as shown in Figure 17, and this confirms the accuracy of the analytical solution for the thin wire model.

Figure 16. Simulated current distribution of a quarter-wavelength dipole antenna by FEKO.

3.3. First Wire Model for Handset Antennas

A typical wire model for handset antennas is shown in Figure 18, which consists of three connected branches b_1, b_2 and b_3. The branch b_1 is the main radiation element, and b_2 and b_3 are grounding wires, which simulate the ground plane. The reference directions of the current flow

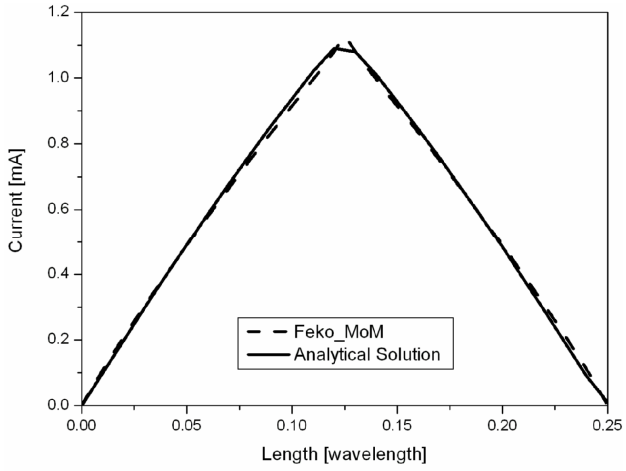

Figure 17. Current distributions for a quarter wavelength dipole.

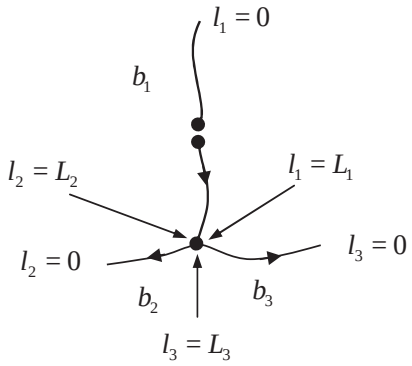

Figure 18. A wire model for the handset antenna.

on each branch are shown in Figure 18. The feeding point is located at branch b_1. The current distributions along b_1, b_2 and b_3 can be written as

$$I_1(l) = \begin{cases} C_1 \cos kl_1 + D_1 \sin kl_1, & l < l_1' \\ C_1' \cos kl_1 + D_1' \sin kl_1, & l > l_1' \end{cases}$$
$$I_2(l) = C_2 \cos kl_2 + D_2 \sin kl_2$$
$$I_3(l) = C_3 \cos kl_3 + D_3 \sin kl_3$$

with the boundary conditions

$$\begin{aligned} I_1(0) &= I_2(0) = I_3(0) = 0 \\ I_1(l_1') &= I_1(l_1') \\ \left.\frac{dI_1}{dl_1}\right|_{l=l_1'^+} &- \left.\frac{dI_1}{dl_1}\right|_{l=l_1'^-} = -j\omega C_0 \\ I_1(L_1) &= I_2(L_2) + I_3(L_3) \\ \phi_1(L_1) &= \phi_2(L_2) \\ \phi_2(L_2) &= \phi_3(L_3) \end{aligned}$$

where ϕ_i is the potential on branch b_i $(i = 1, 2)$. From these boundary conditions, we obtain $C_1 = C_2 = C_3 = 0$ and

$$\begin{aligned} &D_1 \sin kl_1' = C_1' \cos kl_1' + D_1' \sin kl_1' \\ &-kC_1' \sin kl_1' + kD_1' \cos kl_1' - kD_1 \cos kl_1' = -j\omega C_0 \\ &C_1' \cos kL_1 + D_1' \sin kL_1 = D_2 \sin kL_2 + D_3 \sin kL_3 \\ &-kC_1' \sin kL_1 + kD_1' \cos kL_1 = kD_2 \cos kL_2 \\ &kD_2 \cos kL_2 = kD_3 \cos kL_3 \end{aligned}$$

After some manipulations we have

$$\begin{aligned} C_1' &= -j\frac{2\pi}{\eta \ln ka} \sin kl_1' \\ D_1' &= -C_1' \frac{\cos k(L_1 - L_2) \cos kL_3 + \sin kL_1 \cos kL_2 \sin kL_3}{\sin k(L_1 - L_2) \cos kL_3 - \cos kL_1 \cos kL_2 \sin kL_3} \\ &= -C_1' \frac{\cos kL_1 \cos kL_2 \cos kL_3 + \sin kL_1 \sin k(L_2 + L_3)}{\sin kL_1 \cos kL_2 \cos kL_3 - \cos kL_1 \sin k(L_2 + L_3)} \end{aligned}$$

Thus the current distributions on each branch are

$$\begin{aligned} I_1(l) &= \begin{cases} \dfrac{C_1' \cos kl_1' + D_1' \sin kl_1'}{\sin kl_1'} \sin kl_1, & l_1 < l_1' \\ C_1' \cos kl_1 + D_1' \sin kl_1, & l_1 > l_1' \end{cases} \\ I_2(l) &= \frac{-C_1' \sin kL_1 + D_1' \cos kL_1}{\cos kL_2} \sin kl_2 \\ I_3(l) &= \frac{-C_1' \sin kL_1 + D_1' \cos kL_1}{\cos kl_3} \sin kL_3 \end{aligned} \tag{16}$$

Let us consider a three-wire structure shown in Figure 19. The length of each wire is a quarter-wavelength and the feed is located at the

center of one of three wires. The calculated current amplitude on each wire from (16) is compared with the simulated ones using NEC [21]. The results show a very good agreement and are given in Figures 20 and 21, respectively. Due to symmetrical nature of the structure, it can be found that the current amplitudes on the wires W_b and W_c are the same and their maximum amplitude is at half of the maximum amplitude on the excited wire W_a. This result is consistent with the simulated 3D current distribution in Figure 19.

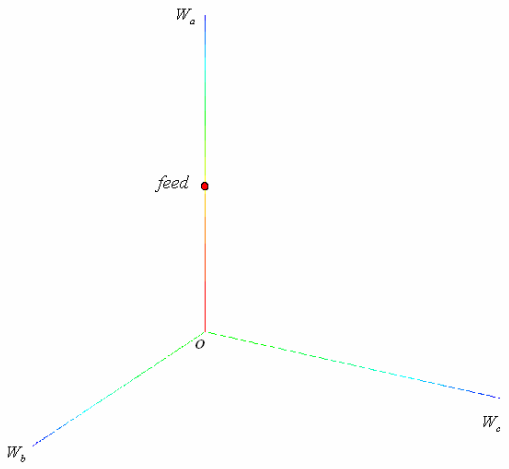

Figure 19. Simulated current distribution on a three wire antenna fed at the center of one of three wires by FEKO.

3.4. Second Wire Model for Handset Antennas

A more reasonable wire model for handset antennas is shown in Figure 22, which consists of branch b_1 of length L_1 and a loop b_2+b_3 of length $L_2 + L_3$. The branch b_1 is the main radiation element, and the loop $b_2 + b_3$ is the grounding wire, which simulates the ground plane. The reference directions of the current flow on each branch are shown in Figure 22. The feeding point is located at $l_1 = l_1'$ of branch b_1. The current distributions along b_1, b_2 and b_3 can be written as

$$\begin{aligned} I_1(l) &= \begin{cases} C_1 \cos kl_1 + D_1 \sin kl_1, & l < l_1' \\ C_1' \cos kl_1 + D_1' \sin kl_1, & l > l_1' \end{cases} \\ I_2(l) &= C_2 \cos kl_2 + D_2 \sin kl_2 \\ I_3(l) &= C_3 \cos kl_3 + D_3 \sin kl_3 \end{aligned} \tag{17}$$

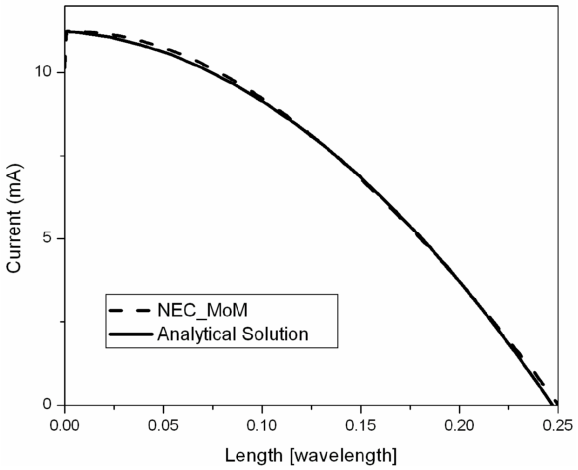

Figure 20. Current distributions on wires W_b or W_c.

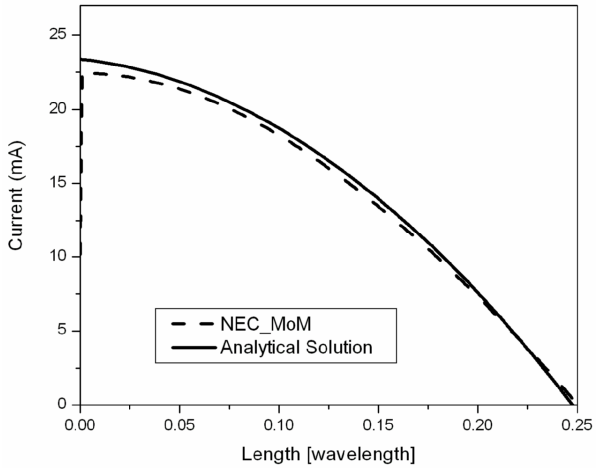

Figure 21. Current distributions on wire W_a.

with the boundary conditions

$$
\begin{aligned}
I_1(0) &= 0 \\
I_1(l_1') &= I_1(l_1') \\
\left.\frac{dI_1}{dl_1}\right|_{l=l_1'^+} - \left.\frac{dI_1}{dl_1}\right|_{l=l_1'^-} &= -j\omega C_0 \\
I_1(L_1) + I_2(L_2) + I_3(L_3) &= 0
\end{aligned}
$$

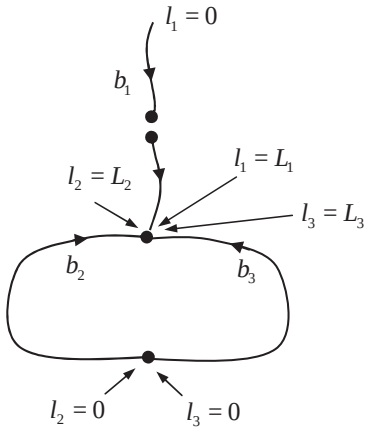

Figure 22. A typical wire model for the handset antenna.

$$\begin{aligned}
\phi_1(L_1) &= \phi_2(L_2) \\
\phi_2(L_2) &= \phi_3(L_3) \\
I_2(0) + I_3(0) &= 0 \\
\phi_2(0) &= \phi_3(0)
\end{aligned}$$

From these boundary conditions, we obtain $C_1 = 0$ and

$$\begin{aligned}
&D_1 \sin kl_1' = C_1' \cos kl_1' + D_1' \sin kl_1' \\
&kC_1' \sin kl_1' - kD_1' \cos kl_1' + kD_1 \cos kl_1' = j\omega C_0 \\
&C_1' \cos kL_1 + D_1' \sin kL_1 + C_2 \cos kL_2 + D_2 \sin kL_2 \\
&\qquad + C_3 \cos kL_3 + D_3 \sin kL_3 = 0 \\
&C_1' k \sin kL_1 - D_1' k \cos kL_1 = C_2 k \sin kL_2 - D_2 k \cos kL_2 \\
&C_2 k \sin kL_2 - D_2 k \cos kL_2 = C_3 k \sin kL_3 - D_3 k \cos kL_3 \\
&C_2 + C_3 = 0 \\
&D_2 = D_3
\end{aligned}$$

After some manipulations we obtain

$$\begin{aligned}
C_1' &= -j \frac{2\pi}{\eta \ln ka} \sin kl_1' \\
D_1' &= C_1' \frac{H_1}{H_2} \\
C_2 &= -\frac{-C_1' \sin kL_1 + D_1' \cos kL_1}{\sin k(L_2 + L_3)} (\cos kL_3 - \cos kL_2)
\end{aligned}$$

$$
\begin{aligned}
C_3 &= \frac{-C_1' \sin kL_1 + D_1' \cos kL_1}{\sin k(L_2+L_3)}(\cos kL_3 - \cos kL_2) \\
D_1 &= \frac{C_1' \cos kl_1' + D_1' \sin kl_1'}{\sin kl_1} \\
D_2 &= -C_2 \frac{\sin kL_2 + \sin kL_3}{\cos kL_3 - \cos kL_2} \\
D_3 &= C_2 \frac{\sin kL_2 + \sin kL_3}{\cos kL_3 - \cos kL_2}
\end{aligned}
$$

where

$$
\begin{aligned}
H_1 &= [\cos kL_1 \cos kL_2 \cos kL_3 - \sin kL_1 \sin k(L_2+L_3)] \sin k(L_2+L_3) \\
&\quad + \sin kL_1 [\cos kL_2 - \cos kL_3]^2 \\
H_2 &= -[\sin kL_1 \cos kL_2 \cos kL_3 + \cos kL_1 \sin k(L_2+L_3)] \sin k(L_2+L_3) \\
&\quad + \cos kL_1 [\cos kL_2 - \cos kL_3]^2
\end{aligned}
$$

To validate the analytical solution in equation (17), let us consider an L-shaped monopole. The ground plane has been simulated with a rectangular loop as shown in Figure 23. The corresponding analytical and numerical results are shown in Figure 24, a good agreement is achieved.

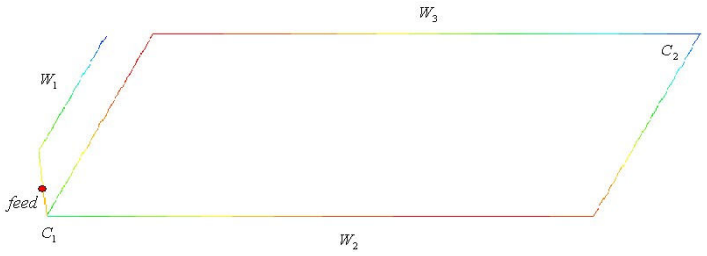

Figure 23. Wire model of a typical handset antenna and the associated 3D current distribution.

4. BANDWIDTH ENHANCEMENT

We now discuss how the antenna parameters and its arrangement influence its bandwidth or quality factor. Notice that in terms of the stored electric energy and magnetic energy and the radiated power from the antenna, a RLC equivalent circuit can be constructed for an

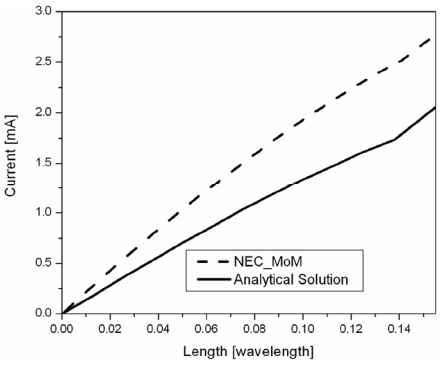

(a)

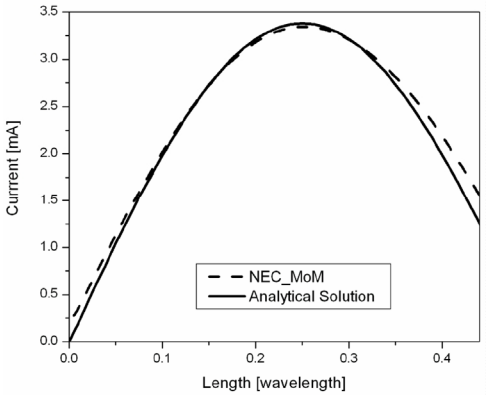

(b)

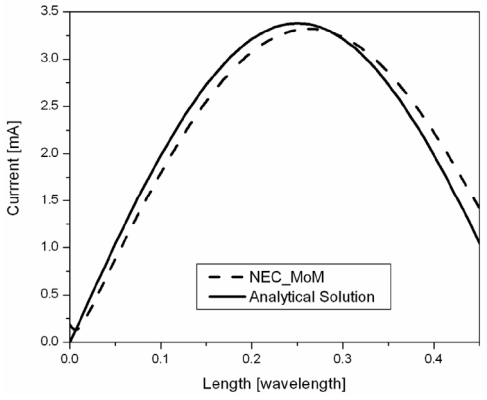

(c)

Figure 24. Current distributions on wires: (a) wire W_1 (b) wire W_2 (c) wire W_3.

ideal antenna, whose element values are defined by [32]

$$R^{rad} = \frac{2P^{rad}}{|I|^2}, \quad L = \frac{4\tilde{W}_m}{|I|^2}, \quad C = \frac{|I|^2}{4\omega^2\tilde{W}_e} \tag{18}$$

where I is the terminal current; P^{rad} is the radiated power; $\tilde{W}_e$ and $\tilde{W}_m$ are the stored electric energy and stored magnetic energy

$$\tilde{W}_e = \frac{1}{8}|I|^2\left(\frac{\partial X}{\partial\omega} - \frac{X}{\omega}\right), \quad \tilde{W}_m = \frac{1}{8}|I|^2\left(\frac{\partial X}{\partial\omega} + \frac{X}{\omega}\right) \tag{19}$$

respectively. In (19), X is the antenna input reactance

$$X = \frac{4\omega\left(\tilde{W}_m - \tilde{W}_e\right)}{|I|^2} = \omega L - \frac{1}{\omega C} \tag{20}$$

The antenna Q is then given by

$$Q = \frac{\omega\left(\tilde{W}_e + \tilde{W}_m\right)}{P^{rad}} = \frac{|I|^2\omega}{P^{rad}}\left[\frac{\tilde{W}_m - \tilde{W}_e}{|I|^2} + \omega\frac{\partial}{\partial\omega}\frac{\left(\tilde{W}_m - \tilde{W}_e\right)}{|I|^2}\right] \tag{21}$$

The calculation of the element values of the equivalent RLC circuit is straightforward [33]. (19) is well known in circuit theory and can be easily derived for a bounded microwave system where the electromagnetic energy is confined in a finite region. In this case the stored electromagnetic energy is simply equal to the total electromagnetic energy for a lossless system. Antenna is an open system, and some of its energy radiates into free space. The total electromagnetic energy around the antenna and the radiated energy into free space are both infinite. But their difference is a finite quantity, which is defined as the stored electromagnetic energy. (19) and (20) indicate that to find the stored energies we only need to know the difference between the stored electric energy and magnetic energy. The difference $\tilde{W}_m - \tilde{W}_e$ can also be determined by making use of the Poynting theorem in the frequency domain

$$\begin{aligned} -\frac{1}{2}\int\limits_{V_0}\overline{\boldsymbol{J}}\cdot\boldsymbol{E}dv(\boldsymbol{r}) &= \frac{1}{2}\int\limits_{\partial V_\infty}\boldsymbol{S}\cdot\boldsymbol{u}_n ds(\boldsymbol{r}) + j2\omega(W_m - W_e) \\ &= P^{rad} + j2\omega\left(\tilde{W}_m - \tilde{W}_e\right) \end{aligned} \tag{22}$$

where the bar indicates the complex conjugate; V_0 is the source region of the antenna; V_∞ is a big region which encloses the antenna; W_m and

W_e are the total average magnetic energy and electric energy stored in the region $V_\infty - V_0$ respectively. Note that in the above equation, we have used the fact that $\tilde{W}_m - \tilde{W}_e = W_m - W_e$ [32]. The left-hand side of (22) can be expressed as

$$-\frac{1}{2}\int\limits_{V_0} \overline{\boldsymbol{J}} \cdot \boldsymbol{E} dv(\boldsymbol{r}) = -\frac{1}{2}\int\limits_{V_0} \overline{\boldsymbol{J}} \cdot (-\nabla\phi - j\omega\boldsymbol{A}) dv(\boldsymbol{r}) \tag{23}$$

where ϕ and $\boldsymbol{A}$ are the scalar and vector potential functions given by

$$\begin{aligned} \phi(\boldsymbol{r}) &= \frac{\eta c}{4\pi}\int\limits_{V_0} \frac{\rho(\boldsymbol{r}')e^{-jkR}}{R} dv(\boldsymbol{r}') \\ \boldsymbol{A}(\boldsymbol{r}) &= \frac{\eta}{4\pi c}\int\limits_{V_0} \frac{\boldsymbol{J}(\boldsymbol{r}')e^{-jkR}}{R} dv(\boldsymbol{r}') \end{aligned}$$

with $R = |\boldsymbol{r} - \boldsymbol{r}'|,\ \eta = \sqrt{\mu_0/\varepsilon_0}$ and $c = 1/\sqrt{\mu_0\varepsilon_0}$. Inserting the above equations into (23) we obtain

$$\begin{aligned} &-\frac{1}{2}\int\limits_{V_0} \overline{\boldsymbol{J}} \cdot \boldsymbol{E} dv(\boldsymbol{r}) \\ &= \frac{\omega\eta c}{8\pi}\int\limits_{V_0}\int\limits_{V_0} R^{-1}\left[c^{-2}\overline{\boldsymbol{J}}(\boldsymbol{r})\cdot\boldsymbol{J}(\boldsymbol{r}') - \overline{\rho}(\boldsymbol{r})\rho(\boldsymbol{r}')\right]\sin(kR) dv(\boldsymbol{r}) dv(\boldsymbol{r}') \\ &+ j\frac{\omega\eta c}{8\pi}\int\limits_{V_0}\int\limits_{V_0} R^{-1}\left[c^{-2}\overline{\boldsymbol{J}}(\boldsymbol{r})\cdot\boldsymbol{J}(\boldsymbol{r}') - \overline{\rho}(\boldsymbol{r})\rho(\boldsymbol{r}')\right]\cos(kR) dv(\boldsymbol{r}) dv(\boldsymbol{r}') \end{aligned} \tag{24}$$

It follows from the above equation and (22) that

$$P^{rad} = \frac{\omega\eta c}{8\pi}\int\limits_{V_0}\int\limits_{V_0} R^{-1}\left[c^{-2}\overline{\boldsymbol{J}}(\boldsymbol{r})\cdot\boldsymbol{J}(\boldsymbol{r}') - \overline{\rho}(\boldsymbol{r})\rho(\boldsymbol{r}')\right]\sin(kR) dv(\boldsymbol{r}) dv(\boldsymbol{r}') \tag{25}$$

$$\begin{aligned} \tilde{W}_m - \tilde{W}_e = \frac{\eta c}{16\pi}\int\limits_{V_0}\int\limits_{V_0} R^{-1}&\left[c^{-2}\overline{\boldsymbol{J}}(\boldsymbol{r})\cdot\boldsymbol{J}(\boldsymbol{r}') - \overline{\rho}(\boldsymbol{r})\rho(\boldsymbol{r}')\right] \\ &\times \cos(kR) dv(\boldsymbol{r}) dv(\boldsymbol{r}') \end{aligned} \tag{26}$$

Thus once the current distribution is known the calculation of the energy difference is simply an integration. When the frequency is very low the calculation of the frequency derivative appearing in (19) is

becoming a challenging task due to the numerical errors. Fortunately alternative expressions for the stored energies of small antennas have been derived to get rid of the frequency derivative [35]

$$\tilde{W}_e = \frac{c\eta}{16\pi}\int\limits_{V_0}\int\limits_{V_0}\frac{1}{R}[\rho(\boldsymbol{r})\overline{\rho}(\boldsymbol{r}')]dv(\boldsymbol{r})dv(\boldsymbol{r}')$$

$$\tilde{W}_m = \frac{c\eta}{16\pi}\left[\frac{1}{c^2}\int\limits_{V_0}\int\limits_{V_0}\frac{\boldsymbol{J}(\boldsymbol{r})\cdot\overline{\boldsymbol{J}}(\boldsymbol{r}')}{R}dvdv' + \frac{k^2}{2}\int\limits_{V_0}\int\limits_{V_0}R\rho(\boldsymbol{r})\overline{\rho}(\boldsymbol{r}')dvdv'\right]$$

Note that the stored energies are always positive. The total energy is then given by

$$\tilde{W}_e + \tilde{W}_m = \frac{c\eta}{16\pi}\left[\frac{1}{c^2}\int\limits_{V_0}\int\limits_{V_0}\frac{\boldsymbol{J}(\boldsymbol{r})\cdot\overline{\boldsymbol{J}}(\boldsymbol{r}')}{R}dvdv' \int\limits_{V_0}\int\limits_{V_0}\left(\frac{k^2R}{2}+\frac{1}{R}\right)\rho(\boldsymbol{r})\overline{\rho}(\boldsymbol{r}')dvdv'\right] \quad (27)$$

It follows from (21), (25) and (27) that

$$Q = \frac{1}{2}\frac{\int\limits_{V_0}\int\limits_{V_0}\frac{1}{c^2}\frac{\boldsymbol{J}(\boldsymbol{r})\cdot\overline{\boldsymbol{J}}(\boldsymbol{r}')}{R}d\Gamma d\Gamma' + \int\limits_{V_0}\int\limits_{V_0}\left(\frac{k^2R}{2}+\frac{1}{R}\right)\rho(\boldsymbol{r})\overline{\rho}(\boldsymbol{r}')dv(\boldsymbol{r})dv(\boldsymbol{r}')}{\int\limits_{V_0}\int\limits_{V_0}\left[\frac{1}{c^2}\frac{\overline{\boldsymbol{J}}(\boldsymbol{r})\cdot\boldsymbol{J}(\boldsymbol{r}')}{R} - \frac{1}{R}\overline{\rho}(\boldsymbol{r})\rho(\boldsymbol{r}')\right]\sin(kR)dv(\boldsymbol{r})dv(\boldsymbol{r}')} \quad (28)$$

It has been shown that the antenna fractional bandwidth is approximately the inverse of the antenna Q [32]. To enhance the antenna bandwidth, we need to reduce the antenna Q, which can be achieved by letting the metal antenna occupy the space as efficiently as possible. For the wire antenna, bending the wires is an efficient way to enhance the bandwidth. To demonstrate this point, let us consider a dipole antenna, a folded dipole antenna, and a circular loop antenna shown in Figure 25. All three antennas have the same maximum dimension $2b$ with wire radius a. The fractional bandwidths for the dipole, folded dipole and loop can be determined from (28) and are

$$B_{dipole} = \frac{(kb)^3}{6\ln(b/a)}, \quad B_{folded\ dipole} = \frac{2(kb)^3}{6\ln(b/a)}, \quad B_{loop} = \frac{\pi(kb)^3}{6\ln(b/a)}$$

respectively [35]. Thus we have $B_{dipole} < B_{folded\ dipole} < B_{loop}$. The above examples are a simple illustration that properly bending the wires can enhance the antenna bandwidth.

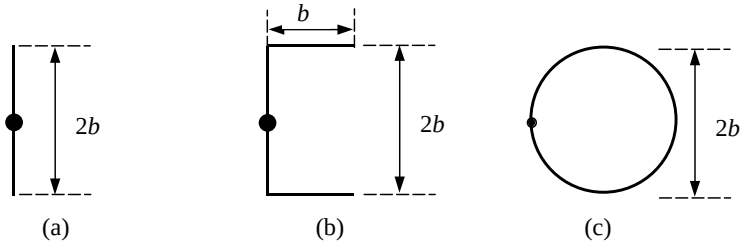

Figure 25. Enhancement of bandwidth: (a) dipole (b) folded dipole (c) loop.

5. THREE DIMENSIONAL MONOPOLE ANTENNA

In the following we introduce three practical examples [22–24], illustrating how the bending strategy can be used to the design of small handset antennas. Each of these antenna designs has the performance that exceeds the minimum requirements for handset applications. The antenna structures are fabricated using a 2 mm wide metal strip in all three examples. They are supported by a frame assembled from FR4 dielectric material. This frame sits on the $60 \times 90\,\text{mm}^2$ PCB made of FR4 dielectric material with thickness 1.5 mm. All three antennas are excited by a coaxial cable probe and their performance is studied in the chamber to stabilize the environment. The antennas are designed to have a length of approximately a quarter of the wavelength at the lowest frequency of interest. The higher resonating frequency bands appear at electrical lengths equal to portions of the total physical length. The non-resonating parts of the antenna(s) act as matching loads to improve the matching at that frequency of operation. The three antenna designs provide multi-band and wideband performance. The different bending (wrapping) of the wire in each antenna design changes the current distribution on their surface, which controls their radiation properties and enhance the bandwidth. In addition, this wrapping reduces the antenna size significantly, making these antennas a promising candidate for handset applications and for future multi-antenna systems in the handset applications.

5.1. First Antenna Design [22]

The first antenna is fabricated on a $1 \times 1 \times 1\,\text{cm}^3$ dielectric frame, as shown in Figures 26 and 27. The symmetric wrapping of the antenna provides omni-directional radiation patterns as shown in Figure 28. The antenna is a pent-band antenna that covers GSM 800/900/1800/1900 and UMTS 2100, as indicated in Figure 29.

Figure 30 are the current distribution at low and high frequencies on the metal surface of the antenna.

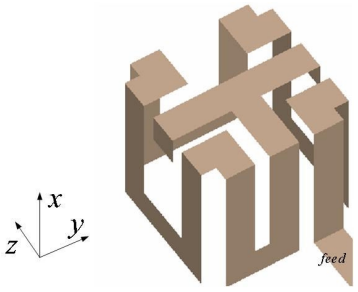

Figure 26. 3D view of the first antenna structure.

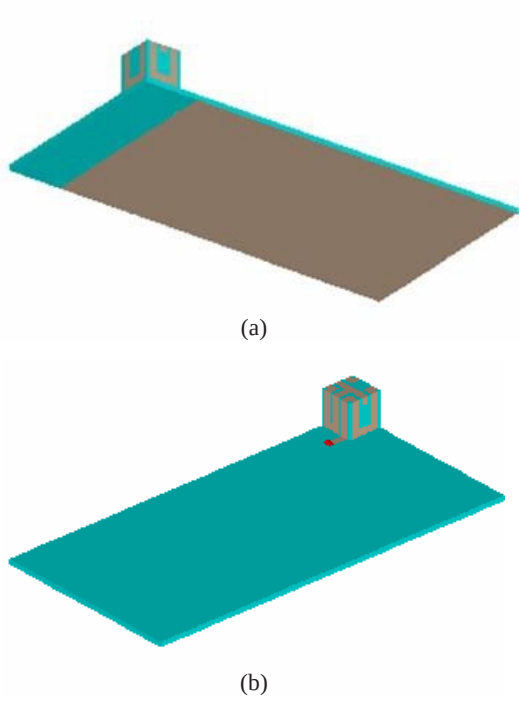

Figure 27. 3D view of the first antenna structure and the supporting frame and board.

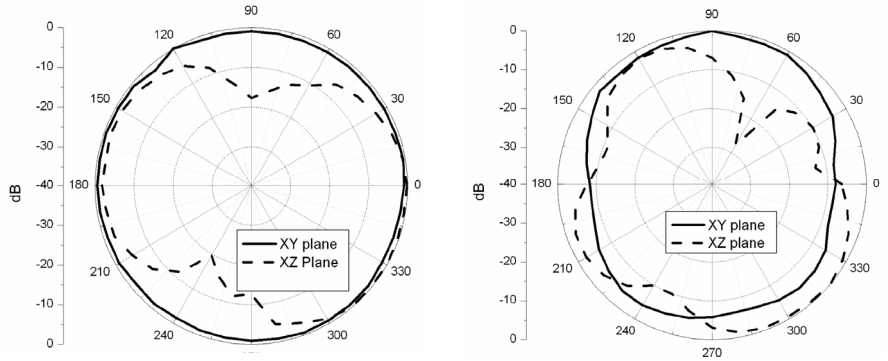

(a) (b)

Figure 28. Measured radiation patterns of the antenna (a) 924 MHz and (b) 1946 MHz.

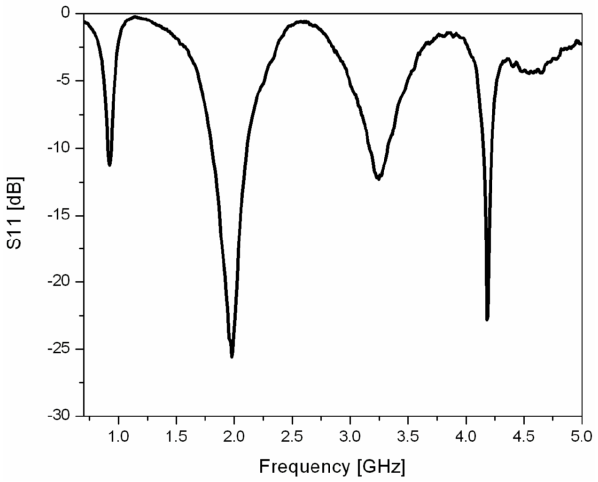

Figure 29. Measured return loss.

5.2. Second Antenna Design [23]

The structure of the second antenna is shown in Figure 31. The antenna is built on a dielectric frame of size $0.7 \times 0.7 \times 1.5\,\text{cm}^3$. A full view of the antenna and the PCB is shown in Figure 32. This antenna is also a pent-band antenna that covers the GSM 800/900/1800/1900 and the UMTS 2100 bands (see return loss shown in Figure 33). The current distributions on the surface of the antenna at different

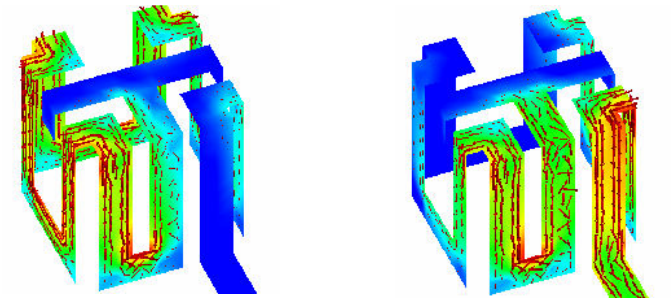

(a) (b)

Figure 30. Simulated current distribution on the surface of the first antenna: (a) 912 MHz (b) 1946 MHz.

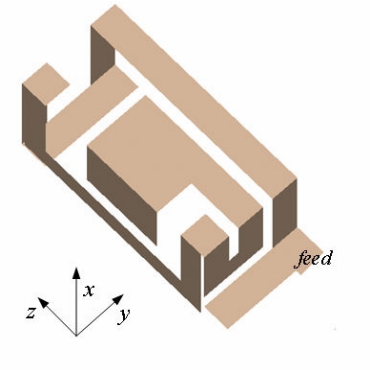

Figure 31. 3D antenna geometry.

frequencies are given in Figure 34, showing how the antenna resonates at each frequency. The corresponding radiation pattern at these frequencies is shown in Figure 35. Notice that this antenna has an almost omni-directional pattern in both measurement planes.

5.3. Third Antenna Design [24]

The structure of the third antenna is shown in Figures 36 and 37. The antenna is built on a frame of size $1.0 \times 0.5 \times 2.5\,\text{cm}^3$. It is a multi-band antenna that covers GSM 800/900/1800/1900, UMTS 2100, and Bluetooth 2400, and its return loss is shown in Figure 38. The current distributions on the surface of the antenna are shown in Figure 39. The radiation patterns are measured and they are shown in Figure 40.

Notice that this antenna has a relatively larger physical size than the first two antennas. Therefore, it is possible here to achieve a

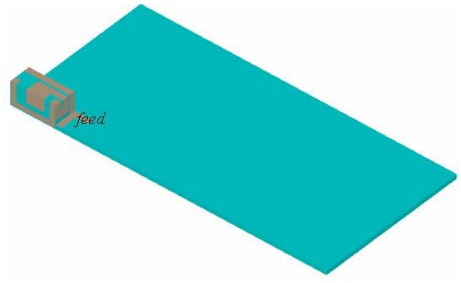

(a)

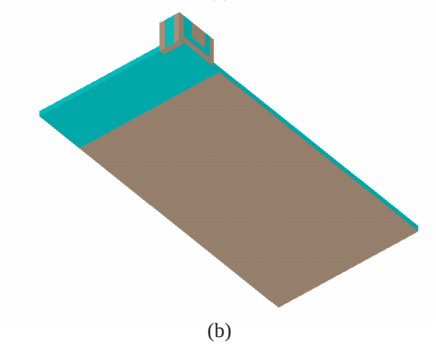

(b)

Figure 32. 3D antenna geometry including the PCB.

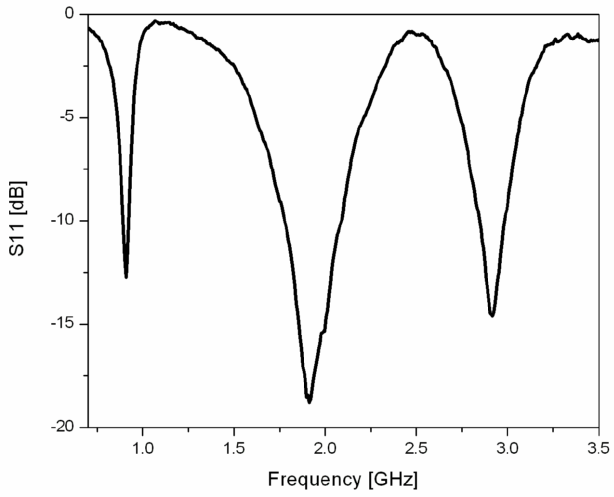

Figure 33. Measured return loss.

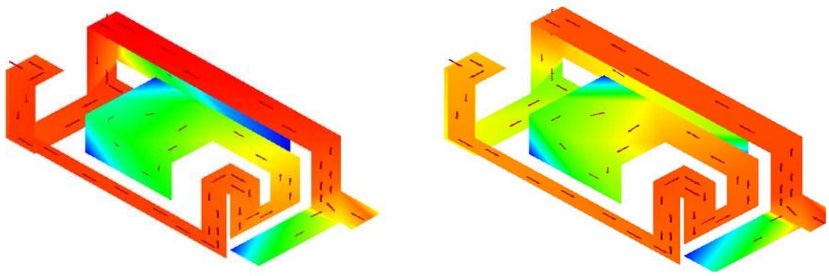

(a) (b)

Figure 34. Current distributions (a) 880 MHz; (b) 1880 MHz.

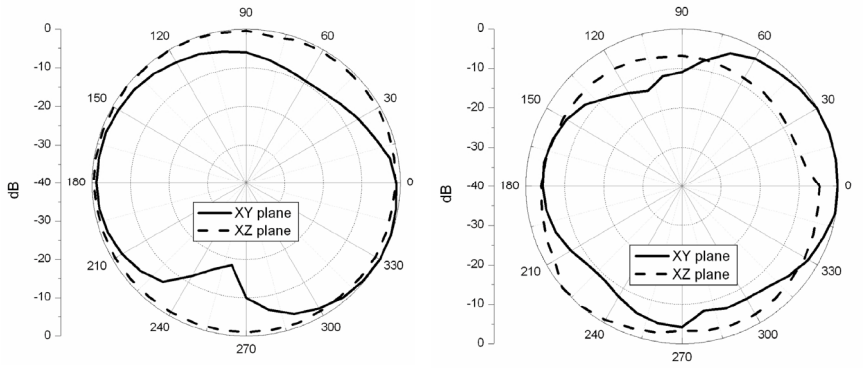

(a) (b)

Figure 35. Measured radiation patterns (a) 880 MHz;(b) 1880 MHz.

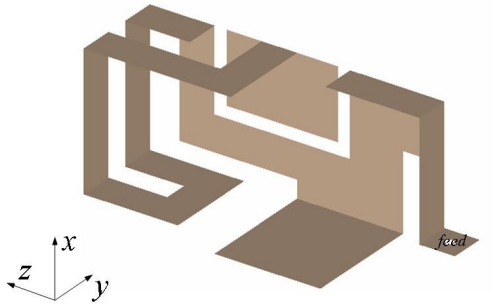

Figure 36. 3D antenna geometry.

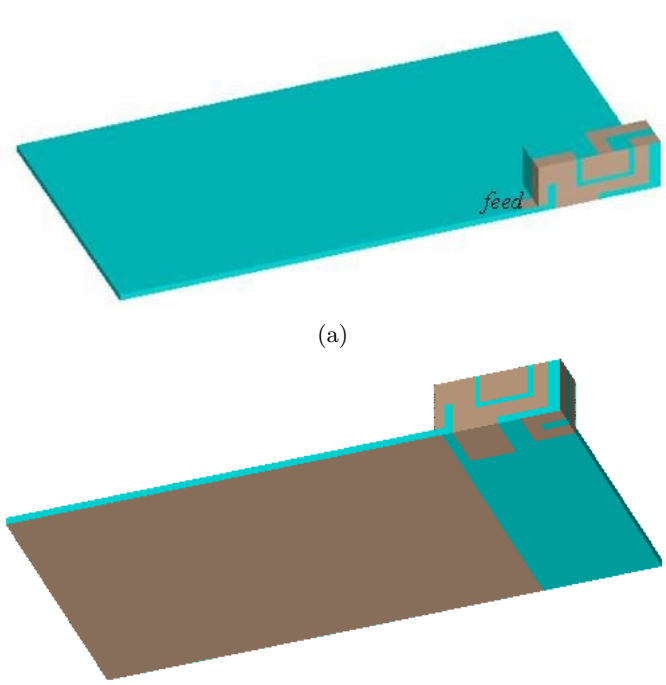

(a)

(b)

Figure 37. 3D geometry of the antenna including supporting frame and ground plane.

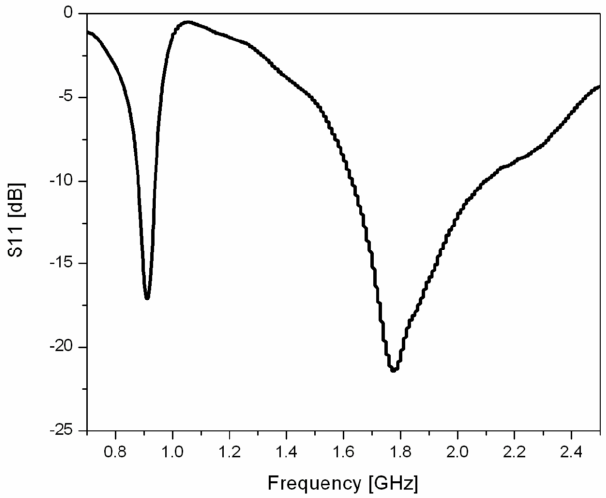

Figure 38. Measured return loss.

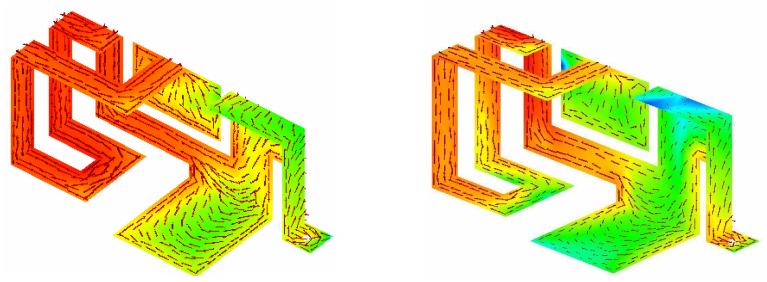

(a) (b)

Figure 39. Current distribution (a) 908 MHz; (b) 1840 MHz.

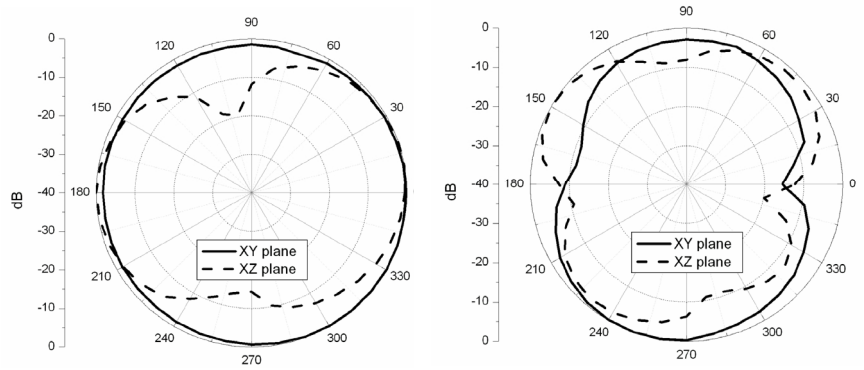

(a) (b)

Figure 40. Measured radiation patterns (a) 908 MHz; (b) 1840 MHz.

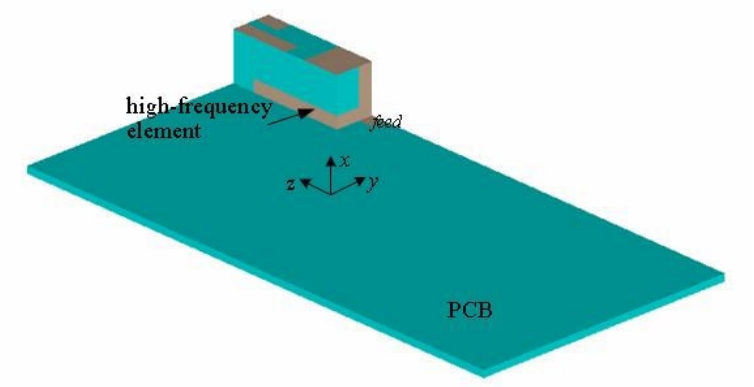

Figure 41. Modified geometry of antenna in Figure 37 to support the high frequency bands in addition to the original frequency bands.

broader bandwidth even at the low frequency range of the GSM 800/900 band. In general, these 3D monopole antenna designs provide broadband performance, and their performance is governed by the size of the antenna [34]. Notice that, given a maximum size, any of our proposed 3D monopole antennas can achieve better performance than a PIFA designed for that same maximum size. In addition, these 3D antenna designs feature the simplicity of the structure and the fast design process.

There are two big challenges in handset antenna designs. The first challenge is how to use a single antenna to cover all the useful frequency bands and the second challenge is how to make the antenna size small enough so that multiple antennas can be deployed in a handset. The 3D monopole antenna designs seem to be the right candidate that can overcome these two challenges at the same time. To illustrate how to make a 3D monopole antenna to cover the most useful frequency bands, let us consider the antenna shown in Figures 36 and 37. We can modify this antenna to make it to cover more frequency bands by adding an additional wire strip with the appropriate length from the feed that would introduce additional resonances at higher frequency ranges. The return loss of the modified antenna is shown in Figure 42, which also covers 802.11a in addition to the original frequency bands. We just mention incidentally that the first challenge can also be overcome by using multi-feed antennas [36, 37].

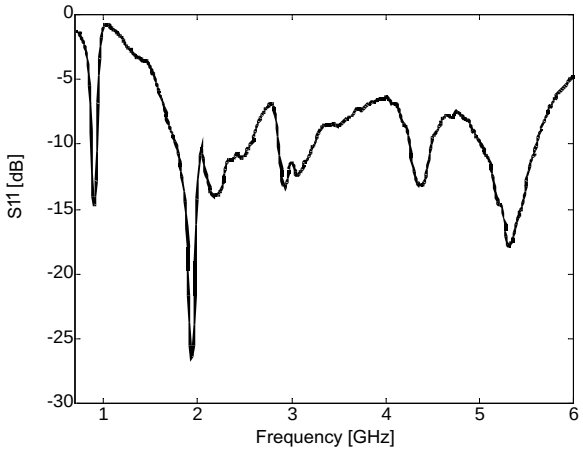

Figure 42. Measured return loss of the modified antenna geometry.

6. CONCLUSION

The handset antenna design is a very difficult process due to the complicated environment. In practice, it is impossible to design a handset antenna with entire environment being taken into account even with the state-of-art simulation tools. The usual procedure is to design the antenna in a simplified environment in which only major components such as PCB and battery are included [38–44]. When the simulated antenna is placed in the real environment, the antenna geometry must be modified to get a reasonable match and radiation performance.

In this paper, we have further simplified the environment by replacing the metal part of the handset antenna with a thin wire model, which is physically possible due to the skin effect. The current distribution on the thin wire model can then be obtained analytically, and the analytical solution so obtained is very close to the current distribution of original handset antenna. This procedure provides an approximate theory that helps explain the handset antenna behavior, and hence, the design procedure, through analytical solutions. The thin wire model represents the backbone of the antenna to be designed. The wire model has simplified the design procedure and reduced the design cycle time and efforts. Numerous analytical and numerical examples are given throughout the paper to validate the theory.

We have used the theory to design three novel wire antennas for handset applications. The design is based on the well-known monopole antenna that is wrapped around a three-dimensional dielectric frame, which results in a three dimensional monopole antenna with a very small maximum size compared to traditional PIFA design. The wrapping or bending controls the radiation patterns and enhances the antenna bandwidth. The performance of the three dimensional monopole antennas is much better than that of a PIFA with the same maximum size. Because of the small size, the proposed three dimensional monopole antennas may be deployed in a handset as antenna elements to form a multiple antenna system, such as a smart antenna array or a multi-input and multi-output (MIMO) system [23, 45, 46].

REFERENCES

1. Yacoub, M. D., *Foundations of Mobile Radio Engineering*, CRC Press, Boca Raton, Feb. 1993.
2. Lécuyer, C., *Making Silicon Valley: Innovation and the Growth of High Tech.*, The MIT Press, Cambridge, MA, Dec. 2005.

3. Fujimoto, K. and J. R. James, *Mobile Antenna Systems Handbook*, Artech House, Norwood, MA, Sep. 2001.
4. Balanis, C. A., "Antenna Theory: A review," *Proceedings of the IEEE*, Vol. 80, No. 1, Jan. 1992.
5. Balanis, C. A., *Antenna Theory: Analysis and Design*, John Wiley and Sons, Inc., Hoboken, NJ, 2005.
6. Wunsch, A. D., "A closed-form expression for the driving-point impedance of the small inverted-L antenna," *IEEE Trans. on Antennas and Propag.*, Vol. 44, 236–242, Feb. 1996.
7. King, R. W. P., J. C. W. Harrison, and D. H. Denton, "Transmission line missile antennas," *IRE Trans. on Antennas and Propag.*, Vol. 8, No. 1, 88–90, 1960.
8. Taga, T. and K. Tsunekawa, "Performance analysis of a built-in inverted-F antenna for 800 MHz band portable radio units," *IEEE Journal on Selected Areas in Comm.*, Vol. 5, No. 5, 921–929, June 1987.
9. Nakano, H., N. Ikeda, Y.-Y. Wu, R. Sukzuki, H. Mimaki, and J. Yamauchi, "Realization of dual-frequency and wide-band VSWR performance using normal-mode helical and inverted-F antennas," *IEEE Trans. on Antennas and Propag.*, Vol. 46, 788–793, June 1998.
10. Tag, T., *Analysis, Design, and Measurement of Small and Low-profile Antennas*, Artech House Publishers, Boston, 1992.
11. Ebrahimi-Ganjeh, M. A. and A. R. Attari, "Interaction of dual band helical and PIFA handset antennas with human head and hand," *Progress In Electromagnetics Research*, PIER 77, 225–242, 2007.
12. Zhang, H.-T., Y.-Z. Yin, and X. Yang, "A wideband monopole with G type structure," *Progress In Electromagnetics Research*, PIER 76, 229–236, 2007.
13. Zhao, G., F.-S. Zhang, Y. Song, Z.-B. Weng, and Y.-C. Jiao, "Compact ring monopole antenna with double meander lines for 2.4/5 Ghz dual-band operation," *Progress In Electromagnetics Research*, PIER 72, 187–194, 2007.
14. Song, Y., Y.-C. Jiao, G. Zhao, and F.-S. Zhang, "Multi-band CPW-FED triangle-shaped monopole antenna for wireless applications," *Progress In Electromagnetics Research*, PIER 70, 329–336, 2007.
15. Eldek, A., "Numerical analysis of a small ultra wideband microstrip-FED tap monopole antenna," *Progress In Electromagnetics Research*, PIER 65, 59–69, 2006.

16. Zaker, R., C. Ghobadi, and J. Nourinia, "A modified microstrip-FED two-step tapered monopole antenna for UWB and WLAN applications," *Progress In Electromagnetics Research*, PIER 77, 137–148, 2007.
17. Liu, Z. D., P. S. Hall, and D. Wake, "Dual-frequency planar inverted-F antenna," *IEEE Trans. on Antennas and Propag.*, Vol. 45, No. 10, 1451–1457, Oct. 1997.
18. Wong, K.-L. and K.-P. Yang, "Modified planar inverted-F antenna," *Electronic Letters*, Vol. 34, 7–8, Jan. 1998.
19. Heald, M. A. and J. B. Marion, *Classical Electromagnetic Radiation*, 3rd edition, Saunders College Publishing, Orlando, FL, 1995.
20. FEKO(r) User Manual, Suite 5.3, Aug. 2006, EM Software & Systems-S.A. (Pty) Ltd, 32 Techno Lane, Technopark, Stellenbosch, 7600, South Africa.
21. Burke, G. J. and A. J. Poggio, "Numerical Electromagnetics Code (NEC) method of moments. Part III: User's guide," Lawrence Livermore National Laboratory, CA, UCID 18834, Jan. 1981.
22. Geyi, W., Q. Rao, and M. Pecen, "Multi-band antenna apparatus disposed on a three dimensional substrate and associated methodology for a radio device," US Patent 32519, pending.
23. Geyi, W., D. Wang, and M. Pecen, "Antenna and associated method for a multi-band radio device," US Patent 32524, pending.
24. Geyi, W., S. M. Ali, and M. Pecen, "Multi-band antenna and associated methodology for a radio communication device," US Patent 32515, pending.
25. Geyi, W., K. Bandurska, and P. Jarmuszewsk, "Antenna with multiple-band patch and slot structures," Patent no: US 7256741, Aug. 14, 2007.
26. Geyi, W., P. Jarmuszewski, and A. Cooke, "Multiple-band antenna with shared slot structure," Patent no: US7239279, July 3, 2007.
27. Geyi, W., P. Jarmuszewsk, and A. Stevenson, "Multiple-band antenna with patch and slot structures," Patent no: US 7224312, May 29, 2007.
28. Geyi, W., P. Jarmuszewski, and A. Cooke, "Multiple-band antenna with shared slot structure," Patent no: US7151493, Dec. 19, 2006.
29. Geyi, W., K. Bandurska, and P. Jarmuszewsk, "Antenna with multiple-band patch and slot structures," Patent no: US 7023387, April 4, 2006.

30. Schelkunoff, S. A., *Antennas: Theory and Practice*, John Wiley & Sons, Inc., 1952.
31. King, R. W. P., *The Theory of Linear Antennas*, Harvard University Press, Cambridge, MA, 1956.
32. Geyi, W., P. Jarmuszewski, and Y. Qi, "Foster reactance theorems for antennas and radiation Q," *IEEE Trans. Antennas and Propagat*, Vol. AP-48, 401–408, Mar. 2000.
33. Geyi, W., "Calculation of element values of antenna equivalent circuit," *Proc. ISAP2005*, 1029–1032, Seoul, Korea, 2005.
34. Geyi, W., "Physical limitations of antennas," *IEEE Trans. on Antennas and Propagat.*, Vol. 51, 2116–2123, 2003.
35. Geyi, W., "A method for the evaluation of small antenna Q," *IEEE Trans. Antennas and Propagat.*, Vol. AP-51, 2124–2129, 2003.
36. Geyi, W., Q. Rao, S. Ali, and M. Pecen, "Mobile wireless communications device with multiple RF transceivers using a common antenna at a same time and related methods," US patent 31351, pending.
37. Geyi, W., Q. Rao, D. Wang, S. Ali, and M. Pecen, "Compact multi-feed multi-band antenna designs for wireless mobile devices," *IEEE Antennas & Propagation Society International Symposium Proceedings*, 1036–1039, June 2007.
38. Elsadek, H. and D. Nashaat, "Ultra miniaturized E-shaped dual band PIFA on cheap foam and FR4 substrates," *J. of Electromagn. Waves and Appl.*, Vol. 20, No. 3, 291–300, 2006.
39. Kuo, L.-C., Y.-C. Kan, and H.-R. Chuang, "Analysis of a 900/1800 MHz dual-band gap loop antenna on a handset with proximate head and hand model," *J. of Electromagn. Waves and Appl.*, Vol. 21, No. 1, 107–122, 2007.
40. Sim, C. Y. D., "A novel dual frequency PIFA design for ease of manufacturing," *J. of Electromagn. Waves and Appl.*, Vol. 21, No. 3, 409–419, 2007.
41. Kouveliotis, N. K., S. C. Panagiotou, P. K. Varlamos, and C. Capsalis, "Theoretical approach of the interaction between a human head model and a mobile handset helical antenna using numerical methods," *Progress In Electromagnetics Research*, PIER 65, 309–327, 2006.
42. Wang, Y. J. and C. K. Lee, "Compact and broadband microstrip patch antenna for the 3G IMT-2000 handsets applying styrofoam and shorting-posts," *Progress In Electromagnetics Research*, PIER 47, 75–85, 2004.

43. Wang, Y. J. and C. K. Lee, "Design of dual-frequency microstrip patch antennas and application for Imt-2000 mobile handsets," *Progress In Electromagnetics Research*, PIER 36, 265–278, 2002.
44. Su, D., D.-M. Fu, and D. Yu, "Genetic algorithms and method of moments for the design of PIFAs," *Progress In Electromagnetics Research Letters*, Vol. 1, 9–18, 2008.
45. Geyi, W., "New magnetic field integral equation for antenna system," *Progress In Electromagnetics Research*, PIER 63, 153–170, 2006.
46. Geyi, W., "Multi-antenna information theory," *Progress In Electromagnetics Research*, PIER 75, 11–50, 2007.